*ACTA ASTRONOMICA*
Vol. **56** (2006) pp. 171–182

# Microlensing of Q2237+0305: Simulations and Statistics

by

M. Jaroszyński and J. Skowron

Warsaw University Observatory, Al. Ujazdowskie 4, 00-478 Warszawa, Poland
e-mail:(mj,jskowron)@astrouw.edu.pl

*Received April 12, 2006*

ABSTRACT

Using Monte Carlo simulations we produce several microlensing amplification maps for each of the four images of the quasar QSO 2237+0305. With FFT algorithms we convolve the maps with the filters representing sources of different sizes and surface brightness distributions. The cuts of the convolved maps represent fragments of synthetic light curves for corresponding sources. Since FFT method is not time consuming we can examine large number of cases and obtain several statistical characteristics of image variability. A simple test involving the measured amplitude of the apparent QSO variability during $\approx 5$ years of OGLE III observations gives an estimate of the relative source velocity, $4000 \pm 2000$ km/s.

**Key words:** *quasars: individual: QSO 2237+0305 – Gravitational lensing*

## 1. Introduction

The quasar Q2237+0305 (the Einstein Cross) (Huchra *et al.* 1985) is the best known example of microlensing induced variability. The variability was discovered by Irwin *et al.* (1989), who were followed by many observers monitoring the four QSO images. The Optical Gravitational Lensing Experiment observations of the source provide the most extensive database covering the seasons 1997–2000 (Woźniak *et al.* 2000a,b) and 2001 to the present, with measurements every few days.

The variability observed in Q2237+0305 can be used to verify models of the source as well as small scale mass distribution in the intervening galaxy. Some limits on the source size and structure and its dependence on the wavelengths considered have been obtained with the help of small amount of observations (Rauch and Blandford 1991, hereafter RB91, Jaroszyński, Wambsganss and Paczyński 1992, hereafter JWP92, Czerny, Jaroszyński and Czerny 1994, Jaroszyński and Marck 1994). The investigation of the influence of the source structure on light curves is still in progress (*e.g.,* Wyithe *et al.* 2000, Yonehara 2001, Wisotzki *et al.* 2003, Moustakas and Metcalf 2003, Chartas *et al.* 2004, to cite a few). In this approach we take the simplified view of Mortonson, Schechter, and Wambsganss (2005), who infer that the source size as measured by the half light radius is the most important parameter of its structure, while the detailed distribution of radiation intensity has only secondary meaning, at least for statistical investigation of light curve properties. While a better knowledge of source models is certainly important in investigation of high magnification events like caustic crossings with detailed observations, the source size alone is sufficient when investigating the relations between variability amplitudes (and similar characteristics) of the different Q2237+0305 images, which is the aim of this paper.

A direct modeling of the microlensing variability of the Q2237+0305 images is a very difficult and time consuming task. Such approach has been applied with success by Kochanek (2004) to the OGLE II data (Woźniak *et al.* 2000a,b). Kochanek constructs huge number of Monte Carlo simulated magnification maps with different mass distributions of the microlenses and different ratios between the discrete and smooth mass surface density. Also the relative velocity, source size and shape can vary. The likelihood that simulations reproduce the observed light curves depends on parameter choice, so the latter can be fitted. Another approach to direct modeling (Lee *et al.* 2005) is less general, since it only attempts to define few microlens masses and positions, responsible for particular high magnification events.

In this paper we examine various statistical characteristics of simulated microlensing light curves. The simulations use the parameters of Schneider *et al.* (1988) describing the four images of Q2237+0305 within the macrolens model. While this model fixes the total surface mass density of the lensing galaxy at the positions of images, the amounts of matter in smooth and discrete distributions are not independently restricted and we use different mixtures of the two. The construction of magnification maps by a ray shooting method (*e.g.,* Kayser, Refsdal and Stabel 1986, Paczyński 1986, Wambsganss 1990) is the main computational burden of our approach. The convolution with the source profile using fast Fourier transform (hereafter *FFT*) coded by Press *et al.* (1992) and various characteristics of the simulated light curves are much less time consuming. We are looking for a simple statistical characteristic of the simulated light curves, which depends on the source size and duration of observations, which shows differences between various images of Q2237+0305 and is easy to compare with observational data. We try several approaches calculating magnification histograms (Mortonson *et al.* 2005), autocorrelation of light curves (*e.g.,* Seitz, Wambsganss and Schneider 1994), and the dependence of the variability amplitude on observation time (Gil-Merino *et al.* 2005).

In the next Section we describe the simulations of amplification maps and the methods of obtaining synthetic light curves. Section 3 describes statistical characteristics of the light curves and contains several plots showing their dependence on model parameters. As an example we compare our predictions of variability amplitude for various Q2237+0305 images with (not fully calibrated) observations of OGLE III. The discussion of the prospects of statistical approach to observations of QSO microlensing follows in the last Section.

## 2. Simulations

We use the macrolens model of Schneider *et al.* (1988), which gives the dimensionless surface mass densities $\kappa_i$ and values of shear $\gamma_i$ at the images positions. The surface mass densities of stars $\kappa_{*i} \leq \kappa_i$ are not given by the macrolens model and we consider three different values for each of them: $\kappa_{*i}/\kappa_i \in \{1, 0.5, 0.25\}$, assuming that it is the same for all images. In the simulations we use the microlenses of limited range of masses ($m \in [0.1\ \mathrm{M}_\odot, 1\ \mathrm{M}_\odot]$) with the Salpeter mass function.

We use the standard angular diameter distances in the concordance cosmological model with dimensionless mass density $\Omega_M = 0.3$, cosmological constant $\Omega_\Lambda = 0.7$, and the Hubble constant $H_0 = 70$ km/s$\cdot$Mpc. (For our purposes the precise values of cosmological parameters have no meaning.) For the galaxy redshift $z_L = 0.039$ and the source redshift $z_S = 1.69$, the distances between the observer, lens and the source are $D_{OL} = 152$ Mpc, $D_{LS} = 1607$ Mpc, and $D_{OS} = 1666$ Mpc respectively. For a microlens mass $M$, the Einstein ring angular size is given as

$$\Theta_E = \sqrt{\frac{4GM}{c^2}\frac{D_{LS}}{D_{OL}D_{OS}}} \approx 7\mu\mathrm{as}\sqrt{\frac{M}{\mathrm{M}_\odot}} \qquad (1)$$

and in the source plane it corresponds to $\tilde{\tilde{r}}_E = D_{OS}\Theta_E \approx 0.06\sqrt{M/\mathrm{M}_\odot}$ pc.

In the calculations we employ the standard ray-shooting method (*e.g.*, Kayser *et al.* 1986). We construct microlensing maps with the resolution of 1024 by 1024 pixels, covering a square region in the source plane of angular size 40 $\mu$as, which corresponds to $\approx 0.32$ pc. For the characteristic relative source – lens velocity of 5000 km/s as measured in the source plane, it would take about 64 years to cross the width of the map.

For each QSO image and each choice of surface mass density in stars $\kappa_*$, we repeat simulations 8 times, obtaining 8 different raw microlensing maps, each represented by a matrix $\mathbf{A}(i,j)$. The rays are shot into a region in the lens plane which is much larger than the resulting maps (0.5 mas on a side), which reduces the number of omitted rays (rays, which would arrive at the map region in the source plane after deflection in the lens plane outside the shooting region) to $\approx 1\%$.

The amplification maps for sources of given size and shape are obtained by convolution of the raw maps with the source surface brightness profile, represented by a matrix $\mathbf{I}(i,j)$. As already mentioned above, we follow the conclusion of Mortonson *et al.* (2005) considering only one parameter family of sources with Gaussian shape and different sizes

$$I(x,y) \sim \exp\left(-\frac{x^2+y^2}{2r_s^2}\right) \tag{2}$$

where $r_s$ is the source size parameter. The convolution can be performed with the help of *FFT* algorithm (*cf.* Mortonson *et al.* 2005), denoted here by $\mathcal{F}$ symbol:

$$\mathcal{A} = \mathcal{F}^{-1}\left(\mathcal{F}(\mathbf{A}) * \mathcal{F}(\mathbf{I})\right) \tag{3}$$

where $\mathcal{A}$ stands for a convolved magnification map defined on the grid. The convolved map can be expressed in magnitudes, $\mathcal{M} = -2.5\ \lg(\mathcal{A})$ and by bilinear interpolation one can obtain a two parameter function $\mathcal{M}(x,y)$ extending the map to all locations in the region of original map. The motion of the quasar in the source plane can be represented by paths $(x_J(s), y_J(s))$ – separately for each of the images $J \in \{\mathrm{A,B,C,D}\}$. The parameter $s$ measures the length along the trajectory. The light curve of the image $J$ is given by:

$$m_J(t) = m_0(t) + \mathcal{M}\left(x_J(s(t)), y_J(s(t))\right) \tag{4}$$

where $m_0(t)$ represents the source apparent magnitude one would measure at the absence of lensing.

According to the macrolens model (Schneider *et al.* 1988) all the images are stretched out azimuthally. In our parametrization these are also the directions of the $x$ axes on our magnification maps. Suppose the path of the source relative to the $x$ axis on image A map is denoted $\beta_A$. Due to the relative orientations of images one has approximately (*cf.* Gil-Merino *et al.* 2005) $\beta_C = \beta_A + 90°$, $\beta_B = \beta_A + 180°$, and $\beta_D = \beta_A + 270°$. (Trajectories parallel for opposite images and perpendicular for the next to each other). On the other hand the starting points of source trajectories on different maps are completely unrelated.

## 3. The Properties of the Synthetic Light Curves

We employ a simplified approach neglecting the internal quasar variability, and considering each of the images separately. The properties of the light curves are likely to depend on the duration of observation. To mimic this property we consider simulated paths of the source of different lengths. The longest path we consider equals half of the map side. Such a path can always be placed inside the map if its middle point belongs to the central square region of the map with a side two times shorter than the whole map. We find such paths choosing their middle points at random from the allowed region and giving them direction $\beta_J$. Every path can be subdivided into smaller fragments. We consider paths of lengths in the range $s \in [0.005, 0.16]$ pc and investigate various statistical properties of the associated light curves for each path length separately.

The amplitude of flux changes on a path of defined length is the simplest characteristic of variability. Using our simulations we calculate the probability distribution for observing given flux amplitude. The distributions depend on the path lengths considered, the assumed surface mass density in stars, the image of interest, the path direction, and the source size. The characteristic half-light radius associated with a black hole of mass $\approx 10^9$ $M_\odot$ has the value $r_s \approx 2\times10^{15}$ cm, so it is probably sufficient to consider sources of the sizes $r_s \in [1,4]\times10^{15}$ cm in relation to Q2237+0305. We consider also larger sources, to get better mathematical insight into the problem. Examples of cumulative probability distributions of flux amplitude for some parameter choices are shown in Fig. 1.

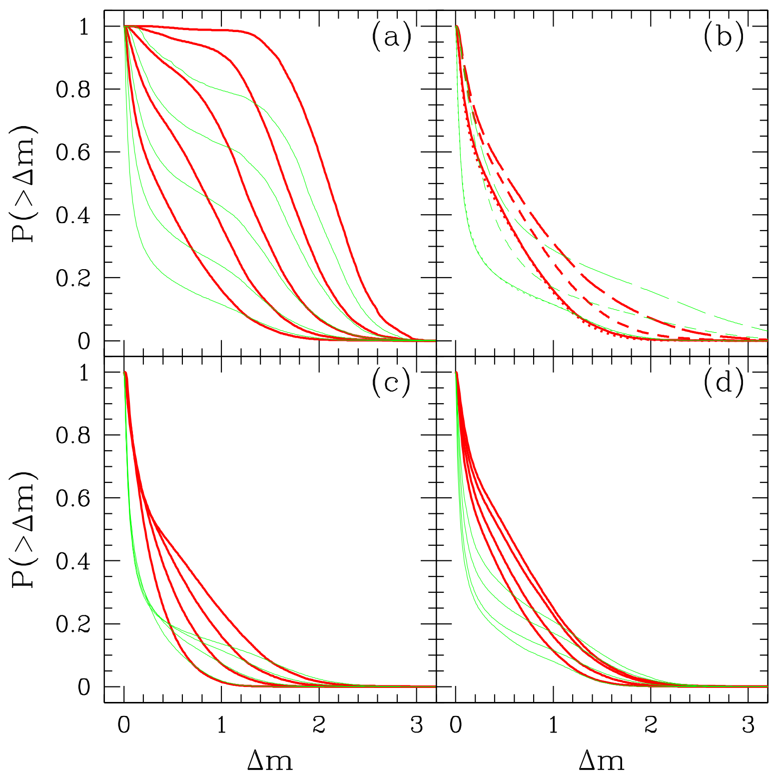


Fig. 1. Cumulative probability distributions for flux amplitude. All panels contain the case corresponding to image A, source path of length $s = 0.02$ pc, the direction $\beta_A = 30°$, and source size $r_s = 2\times10^{15}$ cm. Results for $\kappa_* = \kappa_{\rm tot}$ are shown on all panels with thick lines, and for $\kappa_* = 0.25\kappa_{\rm tot}$ – with thin lines. (*a*) The dependence on path length (for $s \in \{0.01, 0.02, 0.04, 0.08, 0.16\}$ pc – down to top). (*b*) The dependence on image considered (A – solid line, B – dotted, C – short dashed, D – long dashed). (*c*) The dependence on the source size ($r_s = \{1,2,4,8\}\times10^{15}$ cm – top to down). (*d*) The dependence on the path direction ($\beta_A \in \{0°, 30°, 60°, 90°\}$ – down to top).

Inspection of panel (a) shows that the median flux amplitude increases with the path length as expected. The dependence on the image (b) results from the choice of the path directions for the plots. For this particular choice ($\beta_A = 30^\circ$, $\beta_B = 210^\circ$, $\beta_C = 120^\circ$, and $\beta_D = 300^\circ$) the paths C and D meet caustics more frequently as compared to A and B. Different choice of directions may result in different order of the plots. Thus changing the direction one can change the relative amplitudes of flux changes in the pair of images A,B as compared to C,D. The increase of microlensing induced variability with decreasing source size (c) and with increasing angle between the source path and shear direction (d) are also as expected.

We also present probability distributions that a given image of a source of given size, on a path of given length and direction, is magnified by a given amount as compared to the trajectory-averaged value. Examples are shown in Fig. 2.

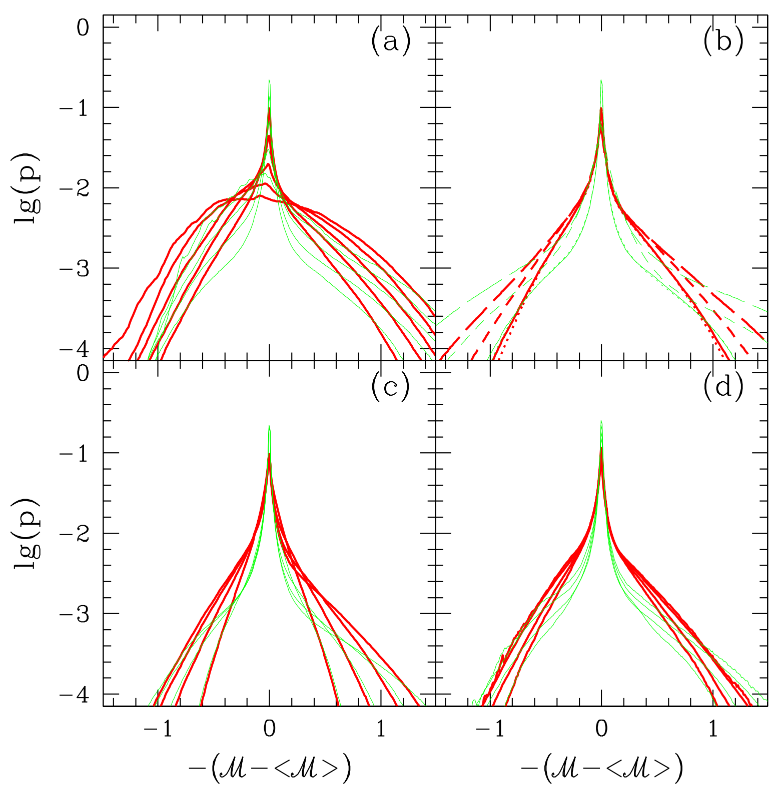


Fig. 2. Probability distributions for excess magnification relative to trajectory-averaged value. (Positive abscissa values correspond to images brighter than average.) The conventions and cases shown are the same as for Fig. 1. The curves plotted correspond to normalized probability distributions; shifting the curves vertically so they all cross the same point at $\mathcal{M} = \langle\mathcal{M}\rangle$ would restore the ordering of plots seen in Fig.1.

There are significant differences between the plots obtained for different model parameter choices, so comparison with magnification distribution of the observed light curves should give at least some limitations on parameters.

Next we examine correlations between magnification values measured on a source path and taken at two points separated by a distance $d$. We define the 1D autocorrelation function for source magnification as:

$$\xi(d) = \frac{\langle \Delta m(s)\ \Delta m(s+d) \rangle}{\langle \Delta m^2 \rangle} \tag{5}$$

where $\Delta m$ here stands for a magnification relative to the average magnification along the path. The averaging in the numerator proceeds with respect to all possible pairs of points with given separation belonging to the considered trajectory, and then with respect to all possible trajectories with given direction on all maps related to given image, and representing magnification for a source of given size. The averaging in the denominator is similar, with all points belonging to a trajectory replacing all pairs. The examples of autocorrelation function dependence on various model parameters are shown in Fig. 3.

The dependence of correlations between source magnification at different points along a trajectory on model parameters is more complicated than for the flux variations amplitude. Panel (c) shows that the dependence on the source size is practically nonexistent (except for $d \leq r_s$). Dependencies on the image, trajectory direction, and mass density in stars are not easy to separate.

The expected change of magnification after traveling a distance $d$ is expressible with the help of autocorrelation function:

$$\langle (m(s+d) - m(s))^2 \rangle = 2\langle \Delta m^2 \rangle\ (1 - \xi(d)) \tag{6}$$

and the above relation is probably the easiest way to obtain the shape of the correlation function from observations. The measurements are done at known instants of time, so the relative source – lens velocity serves as a scaling factor between time and path intervals.

Using the flux amplitude statistics one can try to fit some of the model parameters to actual observations. For fixed source size $r_s$, path length $s$, path direction $\beta_A$, and surface mass density in stars $\kappa_*$, the probability distributions of flux amplitudes $p_J(\Delta m)$ for all four images are given by simulations. We do not show explicitly the dependence of probabilities on parameters which are kept constant to shorten the notation. One can find the most likely values of $\Delta m_J^{\max}$ corresponding to the maxima of their probability distributions. Since the distributions obtained in simulations may not be smooth, and because the observed amplitudes are measured with a typical error of $\delta m \approx 0.1$ mag, it is safer to use filtered quantities. We define the smoothed probability distribution $\tilde{p}_J$ as:

$$\tilde{p}_J(\Delta m) = \int \mathrm{d}\Delta m'\ p_J(\Delta m')\ f(\Delta m', \Delta m) \tag{7}$$

where we use a Gaussian – shaped filter:

$$f(\Delta m', \Delta m) = \exp\left( -\frac{(\Delta m' - \Delta m)^2}{\delta m^2} \right). \tag{8}$$

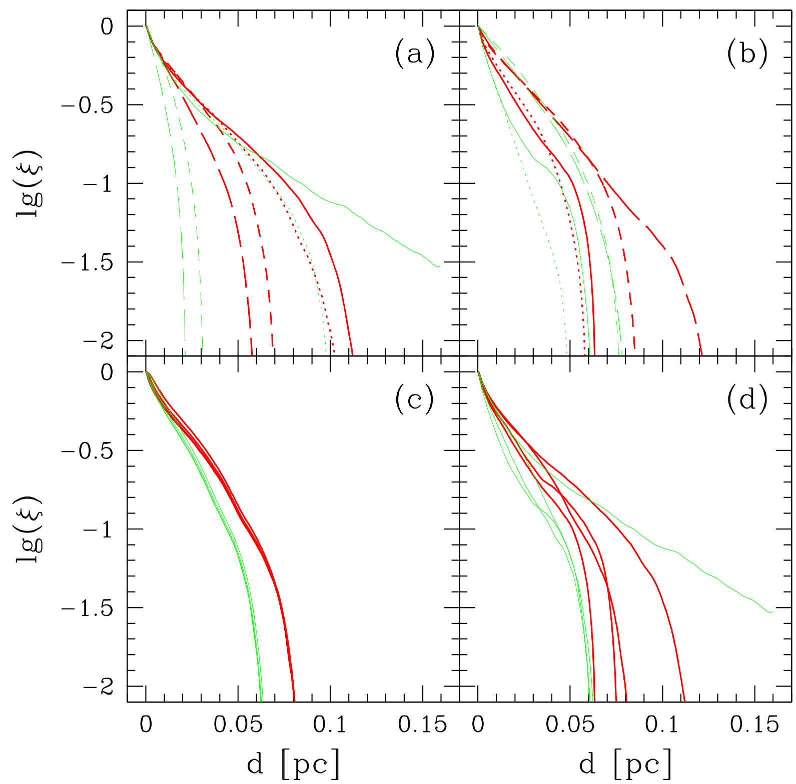


Fig. 3. 1D autocorrelation function for relative source magnification. We use logarithmic ordinate to better separate the plots. Results for $\kappa_* = \kappa_{tot}$ are shown on all panels with thick lines, and for $\kappa_* = 0.25\kappa_{tot}$ – with thin lines. (*a*) The dependence on image considered (A – solid line, B – dotted, C – short dashed, D – long dashed) for $\beta_A = 0°$, and $r_s = 2\times10^{15}$ cm. (*b*) Same as in (a) but for $\beta_A = 90°$. (This time trajectories are perpendicular to shear in A and B, and parallel in images C and D). (*c*) The dependence on the source size ($r_s = \{1,2,4,8\}\times10^{15}$ cm – down to top) for image A and path direction $\beta_A = 30°$. (*d*) The dependence on the path direction ($\beta_A \in \{0°,30°,60°,90°\}$) for image A and source size $r_s = 2\times10^{15}$ cm.

For any set of simulation parameters and measured flux amplitudes $\Delta m_J^{obs}$, one can find the likelihood function:

$$\mathcal{L}(r_s,s,\beta_A,\kappa_*) = \tilde{p}_A(\Delta m_A^{obs})\ \tilde{p}_B(\Delta m_B^{obs})\ \tilde{p}_C(\Delta m_C^{obs})\ \tilde{p}_D(\Delta m_D^{obs}) \qquad (9)$$

where the dependence on simulation parameters is implicit in all the expressions in the RHS. Maximizing likelihood $\mathcal{L}$ gives the best values for parameters.

## 4. An Example: Preliminary Fit to Five Years Amplitude Measurements

To give an example we use the Q2237+0305 light curves obtained by OGLE team in seasons 2001–2006. The data are not fully calibrated yet, and probably would not be useful for more sophisticated tests, but we need only four light curve amplitudes to look for model parameters maximizing the likelihood. Examination of the data gives $\Delta m_J = 0.62$, 1.01, 0.41, and 0.32 for images A, B, C, and D respectively.

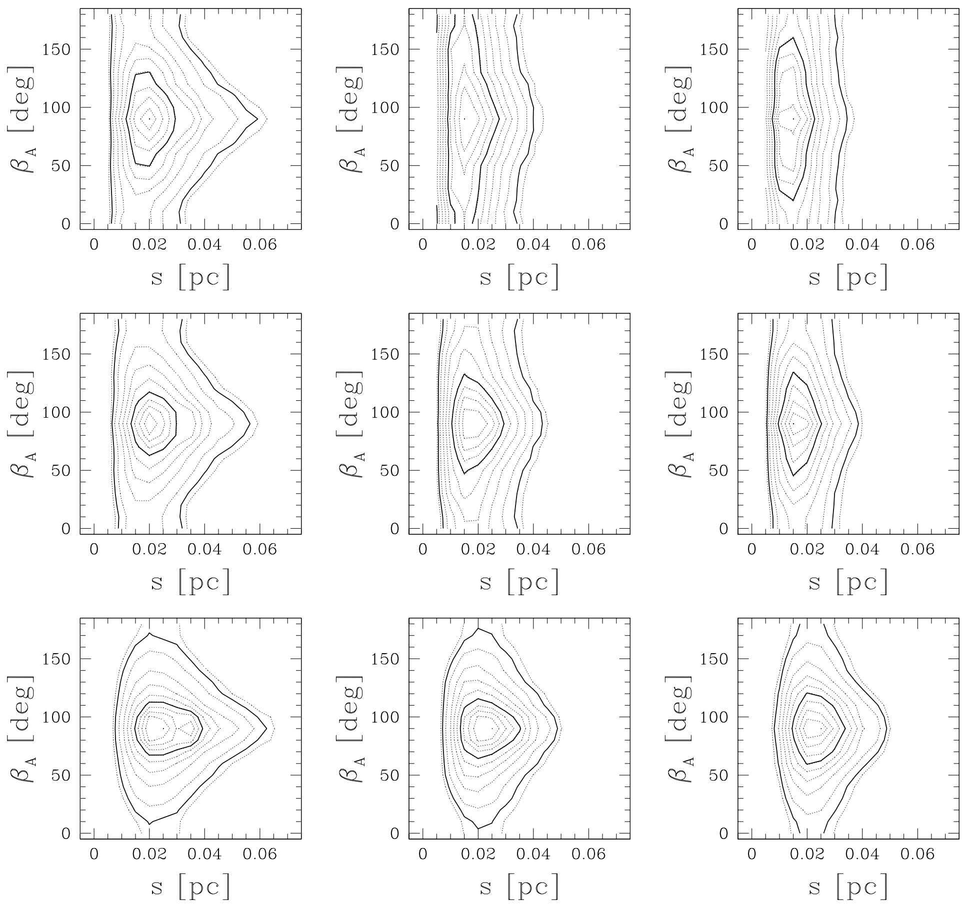


Fig. 4. Low resolution maps of likelihood functions shown in $(s, \beta_A)$ plane for: $r_s = 2 \times 10^{15}$ cm (*upper row*), $4 \times 10^{15}$ cm (*middle row*), $8 \times 10^{15}$ cm (*lower row*), and for: $\kappa_* = 0.25\kappa_{\rm tot}$ (*left column*), $\kappa_* = 0.5\kappa_{\rm tot}$ (*middle column*), and $\kappa_* = \kappa_{\rm tot}$ (*right column*). For each panel the dotted lines correspond to contours drawn at $\{0.1, 0.2, \ldots, 0.9\}$ of the maximum value, and solid lines – to $\{\exp(-0.5), \exp(-2.)\}$ of maximum. The thick contours approximate one and two sigma confidence regions for single parameter estimation.

We follow the procedure described in the previous Section calculating the likelihood function for wide ranges of parameters. We consider path lengths in full range allowed by the size of magnification maps. We include also sources of unreasonably large sizes (up to $30 \times 10^{15}$ cm) to investigate broad sample of models. The path directions are defined by $\beta_A \in [0^\circ, 90^\circ]$, and $\kappa_*/\kappa_{\rm tot} \in \{0.25, 0.5, 1\}$.

For "typical" parameters we obtain synthetic light curves with amplitudes significantly higher than the measured values. For very large source sizes this discrepancy is diminished, since the synthetic light curves are smoothed out. This kind of fit requires, however, unreasonably large source sizes, which are in conflict with the observed fast flux changes. Using the results of early work on the subject (RB91, JWP92) we limit ourselves to sources with $r_s \in \{2,4,8\} \times 10^{15}$ cm. Using these prior values of $r_s$, we explore the likelihood dependence on other parameters.

The number of $\kappa_*$ and $r_s$ values considered is rather limited. We show in Fig. 4 the dependence of likelihood values on the other parameters (path length $s$ and path direction $\beta_A$) for three $\kappa_*$ and three $r_s$ values.

In all cases shown the preferred path direction is given by $\beta_A = 90°$, which means that the variability in images A and B is produced by the source moving perpendicularly to the majority of caustics, and in C and D – in parallel. The dependence of likelihood values on $\beta_A$ is rather weak and in some cases even the one sigma confidence regions reach $0°$. For the path length $s$ the limits are more useful, and the preferred values are only weakly correlated with other parameters. Examination of maps in Fig. 4 gives a rough estimate: $s = 0.02 \pm 0.01$ pc, which corresponds to the source five year travel with the velocity $\approx 4000 \pm 2000$ km/s.

The dependence of likelihood value on surface mass density gives a weak preference to $\kappa_* = \kappa_{\rm tot}$, but other values considered are within one sigma confidence region.

## 5. Discussion

We have obtained several microlensing maps relevant to images A, B, C, and D of Q2237+0305, using the macrolens parameters of Schneider *et al.* (1988). We have considered three possible values of the stars contribution to the surface mass density in the lensing galaxy, $\kappa_*/\kappa_{\rm tot} = 0.25$, 0.5, and 1. We have investigated the microlensing induced variability of the source images related to the source motion along paths of different direction and length. We have also included the dependence of the results on the source size.

We present several statistical characteristics of microlensing induced variability based on the investigation of the synthetic light curves obtained in our simulations. The simplest of all is the dependence of variability amplitude on the direction and length of path traveled by the source. This characteristic can easily be tested – see below. We also present probability distributions of relative magnification of the source on a given path, and the shapes of magnification autocorrelation functions along given direction. The tests involving probability distributions and/or autocorrelations require large amount of well reduced data, and we skip them to the next paper.

We present a simple test confronting the observed and simulated variability amplitudes of the four Q2237+0305 images. For "typical" model parameters the predicted variability amplitudes are larger than measured. It is not excluded, that the real variability is in fact higher, since there are off-seasonal gaps in the observations lasting typically a few months, however we do not consider this possibility to be of high importance.

Formally one may avoid the apparent contradiction considering a very large source. Since the simulated light curves are obtained as convolutions of microlensing maps with source profiles, large sources smooth out the maps lowering the amplitudes of variability. Our fits show, however, that for larger sources the preferred length of source path becomes longer, but the increase is much slower than for the source size. That means that the characteristic time in which the source travels the distance similar to its size is longer, and the short time variability becomes slower, contradicting observations (*e.g.,* RB91). To avoid this contradiction we consider only "small" sources with $r_s \leq 8 \times 10^{15}$ cm (RB91, JWP92). The preferred length of the source path in five years given by our test is $s = 0.02 \pm 0.01$ pc, which corresponds to the source velocity $\approx 4000 \pm 2000$ km/s. Such source velocity can result from $\approx 10$ times slower peculiar motion of the lensing galaxy at $\approx 10$ times shorter distance. This result is in agreement with the upper limit on the lens bulk velocity obtained by Gil-Merino *et al.* (2005) for microlenses of the mass 0.1 $M_{\odot}$.

**Acknowledgements.** We thank Bohdan Paczyński for many helpful discussions and the OGLE Team for kind permission of using their unpublished data. This work was supported in part by the Polish KBN grant 2-P03D-016-24 the NSF grant AST-0204908, and NASA grant NAG5-12212.

## REFERENCES

Chartas, G., Eracleous, M., Agol, E., and Gallagher, S.C. 2004, *Astrophys. J.*, **606**, 78.

Czerny, B., Jaroszyński, M., and Czerny, M. 1994, *MNRAS*, **268**, 135.

Gil-Merino, R., Wambsganss, J., Goicoechea, L.J., and Lewis, G.F. 2005, *Astron. Astrophys.*, **432**, 83.

Huchra, J., Gorenstein, M., Kent, S., Shapiro, I., Smith, G., Horine, E., and Perley, R. 1985, *Astron. J.*, **90**, 691.

Irwin, M.J., Webster, R.L., Hewett, P.C., Corrigan, R.T., and Jedrzejewski, R.I. 1989, *Astron. J.*, **98**, 1989.

Jaroszyński, M., and Marck, J.-A. 1994, *Astron. Astrophys.*, **291**, 731.

Jaroszyński, M., Wambsganss, J., and Paczyński, B. 1992, *Astrophys. J. Letters*, **396**, L65 (JWP92).

Kayser, R., Refsdal, S., and Stabell, R. 1986, *Astron. Astrophys.*, **166**, 36.

Kochanek, C.S. 2004, *Astrophys. J.*, **605**, 58.

Lee, D.W., Surdej, J., Moreau, O., Libbrecht, C., and Claeskens, J.-F. 2005, astro-ph/0503018.

Mortonson, M.J., Schechter, P.L., and Wambsganss, J. 2005, *Astrophys. J.*, **628**, 594.

Moustakas, L.A., and Metcalf, R.B. 2003, *MNRAS*, **339**, 607.

Paczyński, B. 1986, *Astrophys. J.*, **301**, 503.

Press, W.H., Teukolsky, S.A., Vetterling, W.T., and Flannery, B.P. 1992, *Numerical Recipes*, Cambridge: Cambridge Univ. Press.

Rauch, K.P., and Blandford, R.D. 1991, *Astrophys. J. Letters*, **381**, L39 (RB91).

Schneider, D.P., Turner, E.L., Gunn, J.E., Hewitt, J.N., Schmidt, M., and Lawrence, C.R. 1988, *Astron. J.*, **95**, 1619.

Seitz, C., Wambsganss, J., and Schneider, P. 1994, *Astron. Astrophys.*, **288**, 19.

Wambsganss, J. 1990, Ph.D. thesis, Ludwig-Maximilians-Universität (also: MPA550, Max-Planck-Institut für Astrophysik preprint).

Wisotzki, L., Becker, T., Christensen, L., Helms, A., Jahnke, K., Kelz, A., Roth, M.M., and Sanchez, S. F. 2003, *Astron. Astrophys.*, **408**, 455.

Woźniak, P. R., Alard, C., Udalski, A., Szymański, M., Kubiak, M., Pietrzyński, G., and Żebruń, K. 2000a, *Astrophys. J.*, **529**, 88.

Woźniak, P.R., Udalski, A., Szymański, M., Kubiak, M., Pietrzyński, G., Soszyński, I., and Żebruń, K. 2000b, *Astrophys. J. Letters*, **540**, L65.

Wyithe, J.S.B., Webster, R. L., and Turner, E.L. 2000, *MNRAS*, **318**, 762.

Yonehara, A. 2001, *Astrophys. J. Letters*, **548**, L127.